Science of the Total Environment 859 (2023) 160288

Contents lists available at ScienceDirect

Science of the Total Environment

journal homepage: www.elsevier.com/locate/scitotenv

Oceanic and terrestrial origin of precipitation over 50 major world river basins: Implications for the occurrence of drought

Rogert Sorí [a,*], Luis Gimeno-Sotelo [a], Raquel Nieto [a], Margarida L.R. Liberato [b,c], Milica Stojanovic [a,d], Albenis Pérez-Alarcón [a,e], José Carlos Fernández-Alvarez [a,e], Luis Gimeno [a]

[a] Centro de Investigación Mariña, Universidade de Vigo, Environmental Physics Laboratory (EPhysLab), Campus As Lagoas s/n, Ourense 32004, Spain
[b] Escola de Ciências e Tecnologia, Universidade de Trás-os-Montes e Alto Douro, 5001-801 Vila Real, Portugal
[c] Instituto Dom Luiz, Faculdade de Ciências da Universidade de Lisboa, 1749-016 Campo Grande, Portugal
[d] Department of Meteorology and Geophysics, Faculty of Physics, Sofia University "St. Kliment Ohridski", 1164 Sofia, Bulgaria
[e] Departamento de Meteorología, Instituto Superior de Tecnologías y Ciencias Aplicadas, Universidad de La Habana, 10400 La Habana, Cuba

HIGHLIGHTS

- The precipitation recycling and terrestrial moisture export are crucial for tropical and high latitudes basins of Asia.
- Precipitation from oceanic origin is dominant in North American river basins.
- The oceanic and terrestrial components of the precipitation allow attributing the occurrence of drought and its severity.

GRAPHICAL ABSTRACT

River basins and global mechanisms of moisture transport (denoted by arrows).

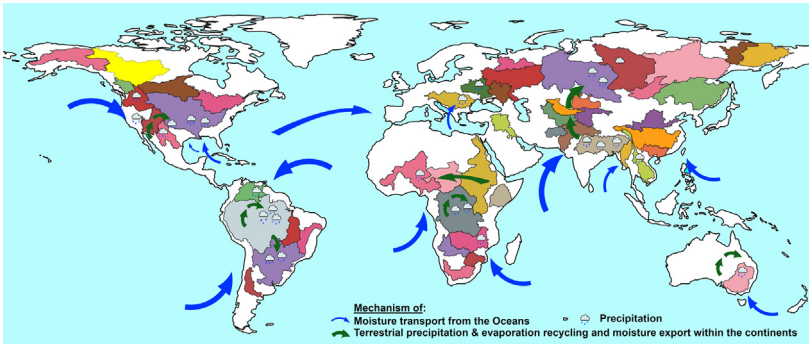

ARTICLE INFO

Editor: Fernando A.L. Pacheco

Keywords:
Precipitation origin
Lagrangian precipitation
River basins
Drought

ABSTRACT

The terrestrial and oceanic origins of precipitation over 50 major river basins worldwide were investigated for the period 1980–2018. For this purpose, we used a Lagrangian approximation that calculates the humidity that results in precipitation from the entire ocean area (ocean component of the precipitation, PLO) and the entire land area (land component, PLT) as well as the sum of both components (Lagrangian precipitation, PL). PL and its components were highly correlated with precipitation over the basins, where PLT accounted for >50 % of the PL in most of them. This confirmed the importance assigned by previous studies to terrestrial recycling of precipitation and moisture transport within the continents. However, the amount of PLO in almost all North American river basins was highlighted. The assessment of drought conditions through the Standardized Precipitation Index (SPI) at a temporal scale of 1- and 3-months revealed the number of drought episodes that affected each river basin, especially the Amazon, Congo, and Nile, because of the lower number of episodes but higher average severity and duration. A direct relationship between the severity of drought episodes and the respective severity computed on the oceanic and terrestrial SPI series was also found for the majority of basins. This highlights the influence of the severity of the SPI of oceanic origin for most basins in North America. However, for certain basins, we found an inverse relationship between the severity of drought and the associated severity according to the SPI of oceanic or terrestrial origin, thus highlighting the principal drought attribution. Additionally, a copula analysis provided new information that illustrates the estimated conditional probability of drought for each river basin in relation to the occurrence of drought conditions of oceanic or terrestrial origin, which revealed the possible main driver of drought severity in each river basin.

* Corresponding author.
E-mail address: rogert.sori@uvigo.es (R. Sorí).

http://dx.doi.org/10.1016/j.scitotenv.2022.160288
Received 10 September 2022; Received in revised form 5 November 2022; Accepted 15 November 2022
Available online 18 November 2022

1. Introduction

The total amount of water that precipitates on large continental regions is supplied by two mechanisms: advection from the surrounding areas external to the region and evaporation and transpiration from the land surface within the region (Brubaker et al., 1993). For instance, although oceans are the most important planetary sources of atmospheric moisture, only approximately 10 % of the evaporated water has been estimated to fall over the continents (Trenberth et al., 2011). However, this percentage makes oceans the primary source of precipitation over continents. The division of land precipitation into oceanic and continental origins has been used in recent years by different methods and datasets. The study of each component separately has revealed crucial information, thus permitting a better understanding of the hydrological cycle on continents (Gimeno et al., 2010, 2012). The importance of oceanic evaporation as a source of continental precipitation under current global warming has also been described (Findell et al., 2019); in particular, oceanic moisture sources were increasingly important for continental precipitation along tropical regions during the period from 1980 to 2016 (Gimeno et al., 2020). However, on average, 40 % of terrestrial precipitation originates from land evaporation and 57 % of all terrestrial evaporation returns as precipitation over land (van der Ent et al., 2010). This highlights the importance of moisture recycling, which is especially high in tropical forest regions, such as the Amazon (Eltahir and Bras, 1994; Zemp et al., 2014) and Congo River basins (Worden et al., 2021). Studies have shown that regional differences in the role of moisture contributions from oceanic or terrestrial origins on the total precipitation are greatly dependent on the geographical location, atmospheric circulation, and other factors, such as orography and land cover characteristics.

Currently, the most important oceanic and terrestrial sources of atmospheric moisture on a global scale are well known (Gimeno et al., 2012). Analyses have also been performed at local and regional scales (e.g., provinces, countries, river basins, and ecological regions) and provided detailed information for understanding the origin of rainfall variability and extreme events. Studies focusing on river basin moisture sources are particularly relevant if we consider that river basins are hydrological units, which means that excluding evaporation, all precipitation that falls remains within the basin to supply rivers and water bodies. Thus, multiple studies have investigated the moisture sources of several world river basins, particularly those that stand out because of their ecological and/or socioeconomic importance. Among the most investigated are the Mississippi in North America, Amazon and Plata in South America, Congo and Niger in Africa, Danube in Europe, Ganges and other river basins located in Southeast Asia, Yangtze in China, and Murray-Darling in Australia. A catalogue available online at http://cola.gmu.edu/wcr/river/basins.html shows the spatial extension of the seasonal climatological sources of moisture for precipitation over 63 major world river basins for the period 1979–2004 as well as their temporal contributions and anomalies. To develop this catalogue, a quasi-isentropic back-trajectory scheme (QIBT; Dirmeyer and Brubaker, 1999; Brubaker et al., 2001) was used, and it treats water vapor as a passive tracer between the time it enters the atmosphere as evaporation and the time it condenses into a cloud and precipitates at the surface. Methodologies based on Eulerian, isotopic, or Lagrangian techniques have also been widely utilised to identify moisture sources, with the latter showing better performance (Gimeno et al., 2012; Winschall et al., 2014). Applying a Lagrangian model for a short study period of four years (1 November 1999 to 30 November 2003), Stohl and James (2005) found that >50 % of the precipitation in 18 of the 39 studied river basins originated over land surfaces, particularly for those located in northern Eurasia (Volga, Dnepr, Don, Ob, Yenisey, and Lena), which are remote from ocean basins. To determine the most important oceanic and terrestrial regions that act as sources of moisture, other studies have also used geographical zones (Martinez and Dominguez, 2014), fixed thresholds for the pattern of moisture uptake (Sorí et al., 2017a), moist-air intrusions (Papritz et al., 2022), and delimited areas of moisture flux divergence (Vázquez et al., 2020). These approaches have the advantage of delimiting the most important sources of moisture; however, a part of the oceanic or terrestrial contribution to precipitation in the region of interest may not be considered. Hence, in this study, we aim to investigate the precipitation of oceanic and terrestrial origin as two separate components of the real precipitation over 50 major world river basins, with oceans and continents considered entirely as sources of moisture, which will provide a better understanding of precipitation variability in these regions.

Extreme dry and wet conditions in any region are driven by different land-atmospheric interactions and have been widely investigated at local, regional, and global scales. The natural variability of the climate system and changes in planetary thermodynamics and atmospheric circulation patterns associated with anthropogenic climate change have been associated with the occurrence and amplification of drought as well as wet periods in certain regions (Cook et al., 2019; Chiang et al., 2021; Pascale et al., 2021; Christidis and Stott, 2021; UNDRR, 2021). Droughts are highly complex to predict and characterise, even with robust instrumental datasets and models (Hao et al., 2018; Vicente-Serrano, 2021; Brunner et al., 2021); hence, the mechanisms associated with this phenomenon are still being investigated. Efforts to understand the occurrence and severity of droughts have included the assessment of the source-sink relationship of atmospheric moisture, which is a better approach than only considering changes in sea surface temperature (SST) and atmospheric circulation. Several studies have confirmed the crucial role of moisture transport from delimited oceanic and terrestrial sources on the occurrence of dry conditions in various river basins, including the Amazon (Drumond et al., 2014; Sorí et al., 2019), La Plata (Martinez and Dominguez, 2014), Paraná (Zandonadi-Moura and Lima, 2018); Congo (Sorí et al., 2017a; Dyer et al., 2017), Niger (Sorí et al., 2019), and Danube (Stojanovic et al., 2017).

Drumond et al. (2019) also confirmed the relationship between the occurrence of meteorological drought episodes in 27 continental regions defined in the Intergovernmental Panel on Climate Change (IPCC) Fifth Assessment Report and the deficit in moisture contribution to precipitation from their respective climatological oceanic and terrestrial sources of moisture. Indeed, recent findings found that 16 % of droughts that affected continents worldwide from 1981 to 2018 were landfalling droughts, which are those that originate over the ocean and “migrates” onto land (Herrera-Estrada and Diffenbaugh, 2020). According to these authors, tracking droughts origin methodologies are in early development in comparison with other attribution techniques employed for extreme precipitation and atmospheric rivers (Guan and Waliser, 2015; Gershunov et al., 2019), or Lagrangian techniques to track the atmospheric pollutants trajectories (Pouyaei et al., 2022; Tso et al., 2022). In this study we use a Lagrangian estimated continental precipitation dataset, obtained by a Lagrangian modelling experiment considering the whole ocean and continents separately, to investigate their role in moisture contribution to precipitation and the occurrence and severity of drought conditions over the river basins selected for this study. Previous studies have used the same Lagrangian approach to investigate moisture transport and drought occurrence, confirming its usefulness. However, in this work the objective is to compute a drought index with the precipitation over the basins, and in addition, with the precipitation series attributed to the transport of moisture from the oceans or the continents themselves. In this way, it is possible to estimate the weight of dry conditions of oceanic or terrestrial origin in the occurrence of drought episodes, and the conditional probability of different drought severity conditions. This approach stands out as a novel method for the attribution of droughts and the study of their characteristics.

2. Methods and datasets

2.1. Study regions

A total of 50 river basins located on every continent, from high latitudes to equatorial zones, were selected for this study. These basins are delimited in Fig. 1, along with the annual mean precipitation over the entire continental region. This figure allows us to visually identify catchments with the greatest contrast in pluviometric regime. As expected, most rainfall occurs along tropical river basins, thus highlighting the maxima observed over the Amazon and Orinoco in South America, the Congo in Africa, and the

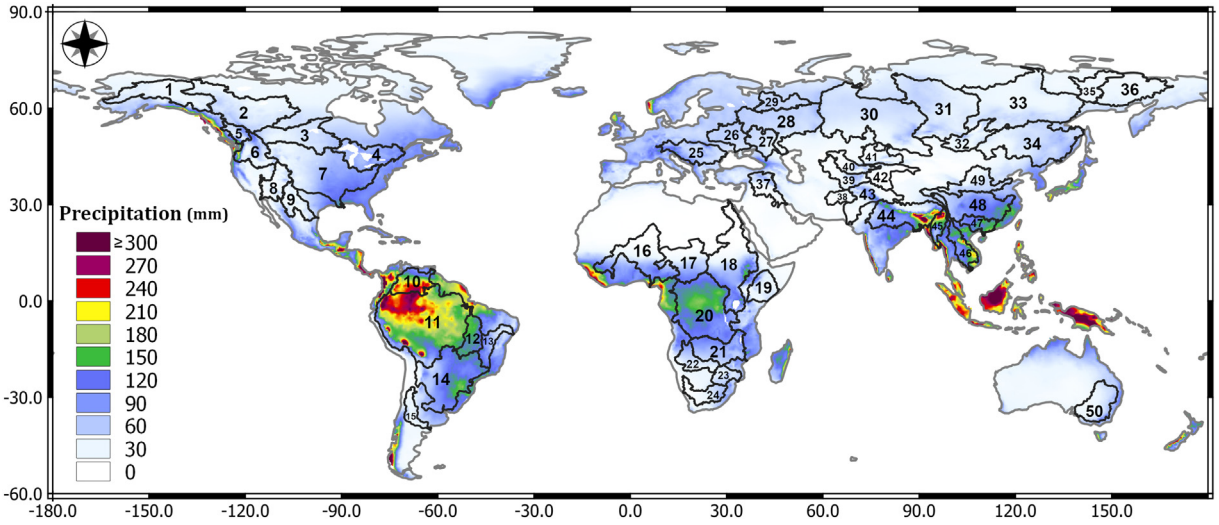

Fig. 1. Geographical location of 50 major river basins worldwide considered in this study, and annual mean precipitation over the period 1980–2018 from the Multi-Source Weighted-Ensemble Precipitation (MSWEP) dataset (Beck et al., 2019).

Ganges, Irrawaddy, and Mekong in Southeast Asia. The topography separates the water that flows into and away from a catchment, thus making it a hydrological unit that interacts with climatic-hydrologic-soil-vegetation factors and morphological factors (Horton, 1932). Many studies have focused on river basins because a large part of the world's population lives in transboundary river basins (TWAP, 2022), while other basins, such as the Amazon and Congo, encompass large forests and host great biodiversity (Wittmann and Junk, 2016; Shapiro et al., 2021), and still others are crucial for the agricultural sector and population food security (Guo et al., 2021). To facilitate the work of this study, these basins are named and numbered by every continent in Table 1.

2.2. Datasets

2.2.1. Precipitation

The monthly gridded values of precipitation from the Multi-Source Weighted-Ensemble Precipitation (MSWEP) dataset v2.8 (Beck et al., 2017, and Beck et al., 2019), P_{MSWEP} hereafter, were used. This is a global precipitation product with data available every 3 h with 0.1° × 0.1° of grid resolution, and available from 1979 to 2020. According to its developers, MSWEP is a unique product because it merges gauge, satellite, and reanalysis data to obtain the highest quality precipitation estimates at every location. Therefore, MSWEP is expected to exhibit better performance than other precipitation products in both densely gauged and ungauged regions. Monthly P_{MSWEP} values were averaged for each watershed for the 1980–2018 study period. Although, this approach may cause the loss of different rainfall characteristics that can occur within the largest river basins, it is correct as river basins are natural hydrological units.

Table 1
List of world river basins selected for this study and their location by continents.

Continent	No	River basin	Continent	No	River basin
North America	1	Yukon	Europe	26	Dnieper
	2	Mackenzie	Asia	27	Don
	3	Saskatchewan-Nelson		28	Volga
	4	St. Lawrence		29	N. Dvina
	5	Fraser		30	Ob
	6	Columbia		31	Yenisey
	7	Mississippi		32	Baikal
	8	Colorado		33	Lena
	9	Rio Grande		34	Amur
South America	10	Orinoco		35	Indigirka
	11	Amazon		36	Kolyma
	12	Tocantins		37	Tigris-Euphrates
	13	San Francisco		38	Helmand
	14	La Plata		39	Amu Darya
	15	Colorado-SA		40	Syr Darya
Africa	16	Niger		41	Ili
	17	Lake Chad		42	Tarim
	18	Nile		43	Indus
	19	Jubba-Shebelle		44	Ganges-Brahmaputra
	20	Congo		45	Irrawaddy
	21	Zambezi		46	Mekong
	22	Okavango		47	Si
	23	Limpopo		48	Yangtze
	24	Orange		49	Hwang Ho
Europe	25	Danube	Australia	50	Murray-Darling

2.2.2. Lagrangian precipitation

The monthly gridded values of Lagrangian precipitation (PL) and their oceanic (PLO) and terrestrial (PLT) components proposed by Nieto and Gimeno (2021) for the period 1980–2018 were used in this study. PLO and PLT were used to analyse the role of precipitation originating from global terrestrial and oceanic sources on the total precipitation over the river basins. These datasets have a spatial resolution of 0.25° × 0.25° in latitude and longitude and were calculated considering the monthly optimum integration times to represent the monthly values of Lagrangian precipitation, which is an advantage over the previous version of Nieto and Gimeno (2019), who used climatological optimum integration times. PL, PLO, and PLT were calculated using global modelling outputs from the Lagrangian particle dispersion model (FLEXPART v9.0) (Stohl and James, 2004; Frank et al., 2005). These outputs were also used to perform a backward experiment from each river basin, and identify the most important regions from where air masses gain humidity before reach the basins.

According to Nieto and Gimeno (2019), the modelling experiment with FLEXPART began by considering the atmosphere divided into approximately 2 million parcels with a resolution of 1° and input data every 6 h and at 61 vertical levels of the atmosphere from the ERA-Interim Reanalysis project (Dee et al., 2011) to force the model. These authors performed a forward-in-time experiment that considered the world separated into two large sources: the entire continental area and the entire ocean extension. In the forward analysis, changes in the specific humidity corresponding to each parcel were calculated at 6-h intervals for 0.25° × 0.25° interpolated resolution, the values of which were vertically integrated to obtain the total budget of (E–P), where E and P represent evaporation and precipitation, respectively. The negative values of this budget are considered to contribute to the precipitation and freshwater supply to the surface. Thus, the values of (E–P) < 0 in the forward experiment from the oceans (continents) are assumed to be a contribution from the oceans (continents) to the continental

precipitation that best correlated with a reanalysis dataset for the optimum integration times (Nieto and Gimeno, 2021). Lagrangian precipitation of oceanic and terrestrial origin are named PLO and PLT, respectively, and the sum of both is termed as the "precipitation calculated by Lagrangian method" (PL), which is an approximation of the precipitation.

2.3. Methodology

2.3.1. Identification of the main moisture sources

The global outputs from the model FLEXPART v9.0 were used to perform a backward in time experiment to identify those regions from where air masses gain humidity before reaching the river basins. The model considered the atmosphere divided into approximately 2 million parcels with a horizontal resolution of 1° in longitude and latitude, later interpolated to 0.25°, and 61 vertical levels. In this analysis, the air masses residing over the basins were tracked backwards in time, calculating every 6 h the changes of specific humidity of the parcels, according to the budget of the (e–p), where e and p represent the evaporation and the precipitation on the parcels respectively. Integrating the (e–p) in the vertical column is obtained the surface freshwater changes according to the budget of (E–P). According to Stohl and James (2004, 2005), in this process, the mass of the parcels is considered constant. Those regions where air masses gain humidity ((E – P) >0) in their travel to the basins, are considered sources of moisture.

2.3.2. Standardized Precipitation Index (SPI)

The Standardized Precipitation Index (SPI) proposed by (Mckee et al., 1993) was used to identify dry conditions in every river basin using the monthly time series of P_{MSWEP}, PLO, and PLT for every river basin. It can be used to study the occurrence and temporal evolution of dry conditions estimated from precipitation and independently study these conditions that occur because of precipitation of oceanic and terrestrial origin. This approach increases the applicability of the index, as it provides more realistic information on the occurrence and severity of drought. Calculating the SPI is suggested for long-term record datasets, which we guarantee in this study with a series of 39 years (468 months). Following the recommendation of the developers, the series was fitted to a gamma probability distribution. Subsequently, the SPI series is calculated and transformed into a normally distributed probability density with a mean of zero and standard deviation of unity for the target region. Thus, positive and negative SPI values indicate wet and dry conditions, respectively. The SPI has been widely implemented because it is perhaps the most straightforward index for assessing the impact of water supply through precipitation, and because of its multiscalar characteristics, the SPI has been used to monitor drought impacts on several hydrological, agricultural, and ecological response variables (Vicente-Serrano et al., 2012). However, despite being appropriate to perform this study, a disadvantage of the SPI is that it fails to diagnose the impact of temperature and evapotranspiration on the soil moisture water content and the final wet or dry conditions.

Taking advantage of the multiscalar nature of the index, it was calculated at time scales of one and three months to obtain the series of SPI1-3_{MSWEP}, SPI1-3_{PLO}, and SPI1-3_{PLT}. To clarify the procedure, for the 3-month time scale, the accumulated precipitation from month $i-2$ to month i was summed and attributed to month i. At 1-month, the SPI is comparable with the percentage of normal precipitation for a 30-day period, and at 3-months, it provides a comparison of the precipitation over a specific 3-month period with the precipitation totals from the same 3-month period for all the years included in the historical record (Svoboda et al., 2012). Dry conditions identified through the SPI1 directly reflect precipitation variability, whereas drought conditions identified through the SPI3 reflect short- and medium-term soil moisture conditions. The classification proposed by Agnew (2022) was used for the analysis (Table 2). It establishes different drought categories based on the probability of recurrence rather than on the magnitude of the SPI, thus making it a more rational approach. In addition, a drought episode is identified when the SPI1 falls below zero (onset), reaches the value of −0.84 or less and later returns to positive values. The duration of one episode was computed as the total number of months from the onset until the end of the episode, which was considered as the last month with a negative SPI value before returning to a positive value. The severity was computed as the absolute value of the sum of all SPI values of the episode.

Table 2
Drought categories based on SPI ranges according to Agnew (2022).

SPI	Probability	Category
>0.84	0.2	Humid conditions
> −0.84 and <0.84	0.6	Normal
< −0.84	0.2	Moderately dry
< −1.28	0.1	Severely dry
< −1.65	0.05	Extremely dry

A multiple regression analysis was performed to assess the dependency between the average severity of drought episodes at 1- and 3-months of the SPI_{MSWEP}, and the corresponding severity was calculated with the SPI1-3_{PLT} and SPI1-3_{PLO} series individually. The size of the coefficient for each independent variable indicates the size of the effect of the variable on the dependent variable, and the sign of the coefficient, i.e., positive or negative, reveals the direction of the effect.

2.3.3. Copula analysis

For each pair of variables (SPI_{MSWEP}, SPI_{PLO}) and (SPI_{MSWEP}, SPI_{PLT}), the correlation was examined in terms of Kendall's τ coefficient, which measures the level of dependence between datasets. Afterwards, for each river basin at a 1- and 3-month temporal scale, a copula-based approach was used to estimate the conditional probability of drought occurrence in terms of the SPI computed with MSWEP data (SPI_{MSWEP}) under drought conditions based on the SPI computed with PLO (SPI_{PLO}) and PLT series (SPI_{PLT}). The conditions of drought (SPI < −0.84), severe and extreme drought (SPI < −1.28), and extreme drought (SPI < −1.65) were used as thresholds. Copulas are a popular statistical method for modelling the conditional distribution function of a pair of random variables (Tootoonchi et al., 2022).

In this study, two pairs of variables were considered: (SPI_{MSWEP}, SPI_{PLO}) and (SPI_{MSWEP}, SPI_{PLT}). We use the R platform (R Core Team, 2022), namely, the R package VineCopula (Nagler et al., 2020), to fit seven different types of copulas to the data: the independence copula (also known as the product copula; see Nelsen (2006)), and the Gaussian, Student's *t*, Clayton, Gumbel, Frank, and Joe copulas (see, e.g., Czado, 2019 for theoretical details). The copula parameters are estimated semi-parametrically: the applied method consists of non-parametrically estimating the marginal distributions and then applying a maximum likelihood estimation (see Shemyakin and Kniazev, 2017 for extensive information about statistical inferences on copulas). The model with the lowest Aikake Information Criterion (AIC) value was selected (Akaike, 1974), and the goodness of fit of the model was assessed by means of the statistical test proposed by Huang and Prokhorov (2014), which was implemented in the R package *VineCopula*. This test is based on White's (1982) information matrix equality, and its null hypothesis is that the copula fits the data well.

Regarding the pair (SPI_{MSWEP}, SPI_{PLO}), the selected copula model C with estimated parameter $\widehat{\theta}$ is used to estimate the desired probabilities for each threshold (*thres*) as follows:

$$\widehat{P}(SPI_{MSWEP} < thres \mid SPI_{PLO} < thres) = \frac{C\left(\widehat{F}(thres), \widehat{G}(thres) \mid \widehat{\theta}\right)}{\widehat{G}(thres)}, \qquad (1)$$

where $\widehat{F}$ and $\widehat{G}$ refer to the estimated marginal distributions of SPI_{MSWEP} and SPI_{PLO}, respectively, and $thres \in \{-0.84, -1.28, -1.65\}$. The procedure for calculating $\widehat{P}(SPI_{MSWEP} < thres \mid SPI_{PLT} < thres)$ is completely analogous; in this case, the pair (SPI_{MSWEP}, SPI_{PLT}) is considered instead of (SPI_{MSWEP}, SPI_{PLO}).

3. Results

3.1. PL, PLO and PLT and their relation with P_{MSWEP}

The annual proportion of PLO and PLT was determined and represented as a percentage in Fig. 2 to identify the dominant annual role of each component over the basins. The monthly values of both variables and P_{MSWEP} are shown in Fig. S1. One drawback of considering all continents as sources of moisture is that this approach does not allow for an assessment of the contribution to precipitation of land-based sources that may exist between the basins themselves. However, the benefit of this approach is that it includes the possible contribution of remote terrestrial and oceanic regions. In addition, Figs. S2, S3, S4, S5 and S6 show the pattern of (E–P) > 0 delimited by the percentile 90, and computed in a backward experiment from the basins. Therefore, these figures illustrate the most important oceanic and terrestrial regions that act as sources of moisture for precipitation in the river basins.

As shown in Fig. 2, the annual percentage of PLO (light blue bars) was greater than that of PLT (orange line) in five (Yukon, Fraser, Columbia, Mississippi, and Colorado) of the nine river basins selected for North America, which are mostly located in the west and under the direct influence of moisture transport from the Pacific Ocean and frequent land falling caused by atmospheric rivers. In addition, the Mississippi River Basin, which occupies the central-east United States, directly receives moisture from the Caribbean (Fig. S2) through the Caribbean Low-Level Jet (Wang, 2007; Cook and Vizy, 2010) and the Great Plains (Algarra et al., 2019), which contributes to precipitation. The annual cycles represented in S1 show the major proportion of PLO during the boreal winter months, with an increase in PLT during the summer. Contrary to North America, PLT is the dominant component of PL in the South American river basins studied here, which confirms the crucial role of recycling and moisture transport over the continent. Despite this result, precipitation of oceanic origin has been documented to play a crucial role in the South American monsoon system during the austral summer, and strong moisture transport from the tropical Atlantic Ocean favors a great amount of precipitation over northern and central-northern South America (Carvalho et al., 2011; Vuille et al., 2012; Wanzeler da Costa and Satyamurty, 2016). This is best seen in the San Franciso River Basin, which is located in the northeast (Fig. S1). The great Amazonian forest is crucial for evapotranspiration and recycled precipitation given the importance of precipitation of terrestrial origin (Keys et al., 2016). Indeed, the Amazon also acts as a source of moisture for precipitation over the La Plata region (Martinez and Dominguez, 2014; Yang and Dominguez, 2019).

Among the African river basins selected for this study, only the Jubba-Shebelle, located in East Africa, has a greater average oceanic influence on the contribution to precipitation. In East Africa, precipitation is greatly influenced by the south easterly winds (Somali Low-Level jet) during boreal summer, thereby inducing a direct contribution to precipitation from the Pacific Ocean (Viste and Sorteberg, 2013; Wu and Bedaso, 2022) and a reversal northeast during winter (Levin et al., 2009; Algarra et al., 2019). Although PLO and PLT follow the annual cycle of P_{MSWEP}, the percentage of PLO with respect to the total PL decreases because of the PLT increase (Fig. S1). It has been documented in Central Equatorial Africa for the Congo River Basin, which is home to a dense and humid forest, and its role in precipitation is high (Sorí et al., 2017a; Worden et al., 2021). Other studies have also documented this phenomenon in West Africa, where the West African westerly jet (Pu and Cook, 2010) and the monsoon flow from the Gulf of Guinea (Lélé et al., 2015; Sorí et al., 2017c) play an important role in precipitation in the Niger River Basin. The Sahel contribution to precipitation in this basin is also crucial (Nieto et al., 2006; Yu et al., 2017).

In the Danube Basin, the proportions of PLO and PLT were quite similar; however, in the Dnieper, the percentage of PLT (~62 %) was greater than that of PLO (~38 %). In Asia, the average PLO is only higher than 50 % in the Mekong and Si, which are both located in Southeast Asia and highly affected by the moisture flux from the Indian Ocean, particularly the Bay of Bengal (Fig. S5), during the monsoon season (Zhao et al., 2016; Sorí et al., 2017b; Dey and Döös, 2021). In addition, the monthly percentage of PLO increased during the monsoonal season in the Ganges-Brahmaputra. Keune and Miralles (2019) revealed that approximately 74 % of the summer precipitation over European watersheds depends on moisture supplied from other watersheds, which can explain the high values of PLT, particularly in basins such as Tarim, Ob, Baikal, Syr Darya, Amu Darya, Ili, Lena, and Yenisey. In addition to land-vegetation-atmospheric interactions, the location of the basins and the influence of the atmospheric moisture transport mechanism also determine the amount of precipitation from different sources. For example, the Danube receives a large amount of moisture for precipitation from the Atlantic Ocean and the Mediterranean (Fig. S4), although the terrestrial contribution increases when precipitation increases during the summer months (Ciric et al., 2016).

The time series of P_{MSWEP} was correlated with PL, PLO, and PLT, and the positive and high *r* values indicated that were mostly statistically significant at the 95 % confidence level (Fig. 3). Smaller correlations between P_{MSWEP} and PL were obtained for the Mississippi, Colorado, Fraser, and St. Lawrence River basins in North America; Orinoco in South America; Lake Chad, Congo, Jubba-Shebelle, and Orange in Africa; and Syr Darya and Ili

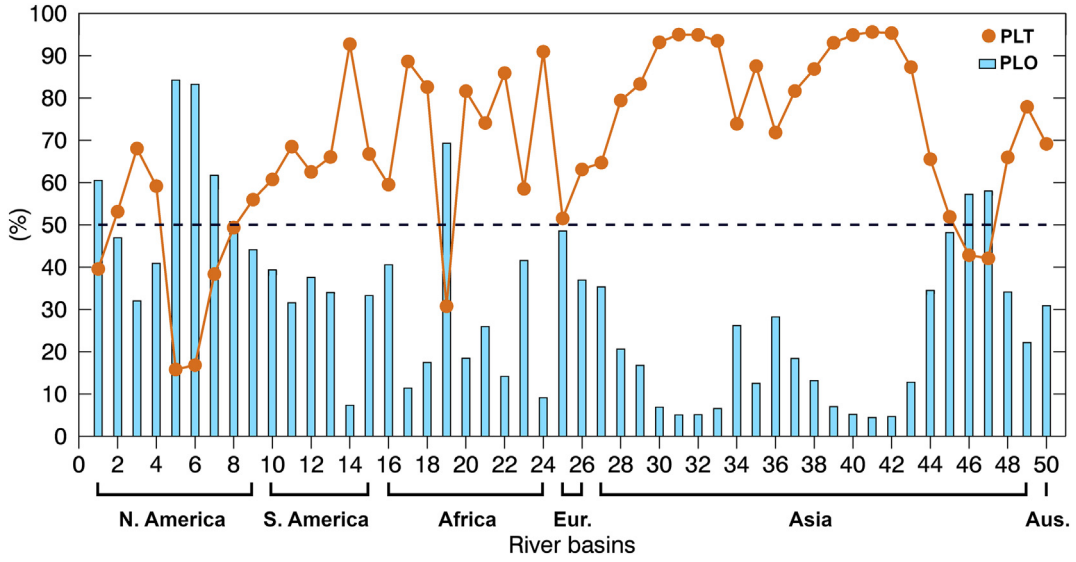

Fig. 2. Average PLO (light blue bars) and PLT (orange line) by river basin expressed as a percentage and ordered as shown in Table 1. Period 1980–2018.

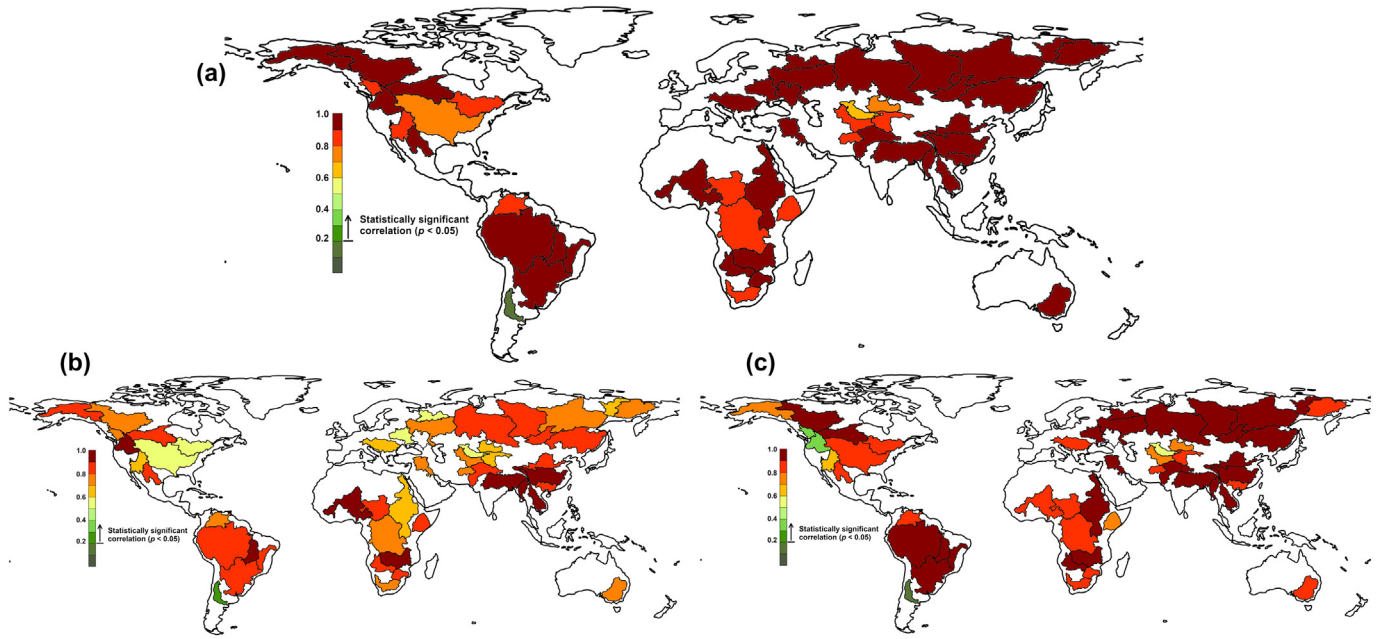

Fig. 3. Correlation coefficient of P_{MSWEP} with PL (a), PLO (b) and PLT (c). Period 1980–2018. Statistically significant *r*-values are identified through the *t*-test for $p < 0.05$.

in Asia (Fig. 3a). The overall high linear relationship between P_{MSWEP} and PL is in agreement with previous findings that investigated this relationship, although at a grid scale over continents (Gimeno et al., 2020), thus confirming the usefulness of the modelled PL in the study of precipitation variability over continents. In addition, correlations between P_{MSWEP} and PL components (PLO and PLT) were calculated to identify which components have a stronger relationship with precipitation variability. The relationships were also high and statistically significant but slightly decreased for some basins, as shown in Fig. 3b and c, respectively. In North America, higher correlations with PL and PLO (Fig. 3a, b) were obtained for the western basins Conversely, the lowest correlations between P_{MSWEP} and PLO were obtained for the Mississippi and St. Lawrence River basins, although, these were statistically significant. Correlations with PLT were higher in the eastern basins of North America (Fig. 3c). In South America, the correlations obtained between P_{MSWEP} and PLO (Fig. 3b) were also mostly high, with the major association obtained for the Tocantins River Basin and a lower and non-statistically significant obtained for the Colorado-SA River Basin. With PLT, the correlation increased, particularly for the Amazon, La Plata, Tocantins and San Francisco (Fig. 3c). In Africa, the relationship between PLO and precipitation in every basin is high, especially for Niger and Zambesi, while with PLT, the correlation increased for the Nile, Congo, Okavango, and Orange (Fig. 2c).

In European and Asian river basins, the correlations are generally higher with PLT than with PLO, except for those obtained for the Ganges-Brahmaputra, Irrawaddy, Mekong, and Yangtze, which remain higher than 0.9, as shown in Fig. 3b and c. Southeast Asian river basins are particularly susceptible to receiving a great amount of moisture for precipitation from the Indian Ocean (Fig. S5), particularly during the monsoon season from the Indian Ocean (Sorí et al., 2017b; Yang et al., 2019; Shi et al., 2020). In contrast, northern Eurasia is characterized by major precipitation of terrestrial origin (Figs. 2, S5), which seems to play a crucial role in the relationship with the total precipitation time series in the basins (Fig. 3c). The correlation between P_{MSWEP} and PLT was also higher than that with PLO for the Murray-Darling River Basin in Australia, which suggests the importance of the recycling process within this continent.

3.2. Identification of dry conditions

SPI1-3_{MSWEP}, SPI1-3_{PLO}, and SPI1-3_{PLT} were calculated for each basin for the study period 1980–2018. The large temporal variability and number of basins make it difficult to represent each series. However, to show the temporal occurrence of dry and wet conditions, we display in Fig. S7 the $SPI3_{MSWEP}$ for February, May, August, and November, which permits the characterization of the seasonal dry/wet conditions in each river basin.

The total number of drought episodes according to the SPI1-3_{MSWEP} that affected each river basin during the study period was identified and is presented in Fig. 4a and b. In addition, the average severity of the episodes was ordered from higher to lower, and their respective average durations appear in Fig. 4c and d. Among the North American river basins studied here, the majority of drought episodes according to the $SPI1_{MSWEP}$ occurred in the Fraser and Saskatchewan-Nelson basins, with 68 and 67 episodes, respectively (Fig. 4a). These were followed by the MacKenzie, Mississippi, and St. Lawrence basins. However, despite being affected by a greater number of episodes, the average severity and duration of these episodes were not greater than those affecting other basins in North America, such as the Columbia and Mississippi (Fig. 4c). In South America, the Amazon stands out because of the lower number of events according to the $SPI1_{MSWEP}$, although in contrast, it is the second basin with the highest average severity and duration of drought episodes at this time scale. The second basin in terms of the average severity and duration of episodes in South America is the Orinoco. A visual analysis of Fig. 4a reveals that the number of drought events in African basins appears to be lower than that in the other river basins. In addition, the number of episodes differs greatly between the Congo River Basin (38) in Central Equatorial Africa and the Orange Basin (59) in South Africa. Indeed, during the study period, the Congo Basin experienced the highest average severity and duration of drought episodes compared with the other basins, while drought episodes in the Orange were, on average, less severe (Fig. 4c). Among the Asian river basins, the Helmand Basin had the lowest number of episodes (43; Fig. 4c). In terms of the major average severity of episodes in the Asian river basins, Lena had the maximum, and Hwang Ho had the minimum. Finally, the Murray-Darling River Basin in Australia was affected by 53 drought episodes according to the $SPI1_{MSWEP}$, with an average severity and duration of 2.81 and 3 months, respectively.

The identification of drought episodes through the $SPI3_{MSWEP}$ (Fig. 4b) shows a drastic reduction in the number of episodes that affected each river basin relative to those obtained with the $SPI1_{MSWEP}$ (Fig. 4a). This is because at a 3-month temporal scale, the variability of the index is lower, thereby reducing the number of flash droughts and thus the number of events. Nonetheless, the Congo Basin was also affected by the lowest

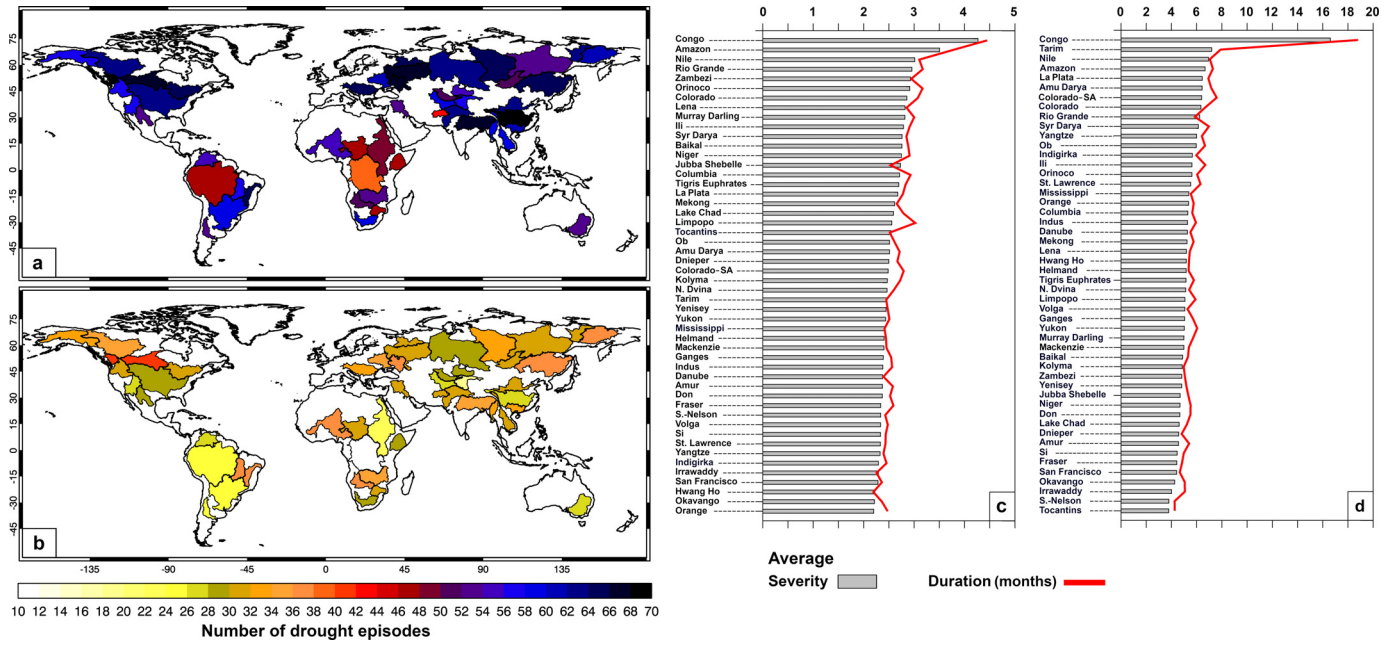

Fig. 4. Total number of drought episodes that affected each river basin according to the $SPI1_{MSWEP}$ (a) and the $SPI3_{MSWEP}$ (b) during the period 1980–2018. The average severity $SPI1_{MSWEP}$ (c) and the $SPI3_{MSWEP}$ (d) drought episodes are ordered from higher to lower (gray bars), and the respective average duration is shown in months (red line).

number of drought episodes, although these events had the highest severity and average duration (Fig. 4d). Similarly, the Amazon, Nile, and Tarim were affected by a few episodes, although they were among the most severe and longest on average. At this time scale, a large number of drought episodes affected the Fraser and Saskatchewan Nelson river basins, both in North America. However, the episodes in both basins were among those with the lowest severity and duration on average.

A multiple regression analysis was performed between the severity of each drought episode at 1 and 3 months of the SPI_{MSWEP} for every basin, and the corresponding severity was calculated using the $SPI1\text{-}3_{PLT}$ and $SPI1\text{-}3_{PLO}$ series. The sizes of the coefficients in the equation are represented as light blue bars for $SPI1\text{-}3_{PLO}$ and as brown filled circles for the $SPI1\text{-}3_{PLT}$ in Fig. 5. Their magnitude indicates the size of influence on the final severity of the episodes identified with the $SPI1\text{-}3_{MSWEP}$, and their sign (positive or negative) of influence.

The regression coefficients of the $SPI1\text{-}3_{PLO}$ and $SPI1\text{-}3_{PLT}$ were positive for all North American river basins (Fig. 5a), thus revealing that both components of PL play a positive role in the severity of drought episodes. $SPI1_{PLO}$ was found to have a major influence on drought episode severity in seven of the nine river basins of North America studied here, while the severity of drought from terrestrial origin plays a major role in the Colorado and Rio Grande. The same analysis was performed for drought episodes at the 3-month temporal scale of the SPI_{MSWEP} (Fig. 5b), and it revealed that the predominant influence of oceanic sources on the severity of drought episodes was maintained, although the terrestrial is dominant in the Colorado Basin. In the South American river basins, the severity of meteorological drought episodes is mostly driven by the severity of the SPI calculated using the PLT series, except for the San Francisco River Basin (Fig. 5a). This basin is the most easterly located, which favors moisture arriving from the tropical Atlantic Ocean in both summer and winter through easterly winds (Montini et al., 2019). Therefore, >50 % of the Lagrangian precipitation results are from oceanic origin (Fig. 2). The Amazon, Tocantins, and Colorado-SA stand out because the severity of the episodes is negatively related to the $SPI1_{PLO}$-associated severity. The severity of drought episodes identified with the $SPI3_{MSWEP}$ is also opposite to the associated $SPI3_{PLO}$ severity in the Orinoco, Amazon, and Tocantins.

In the African river basins, the results were mostly heterogeneous, with the severity of the $SPI1_{MSWEP}$ drought episodes in the Lake Chad, Jubba-Shebelle, Zambezi, and Okavango river basins dominated by the severity of the $SPI1_{PLO}$ and the other basins dominated by the severity of the $SPI1_{PLT}$. Consistent with various studies, this finding confirms that the Congo River Basin dense rainforest in Central Equatorial Africa, which is

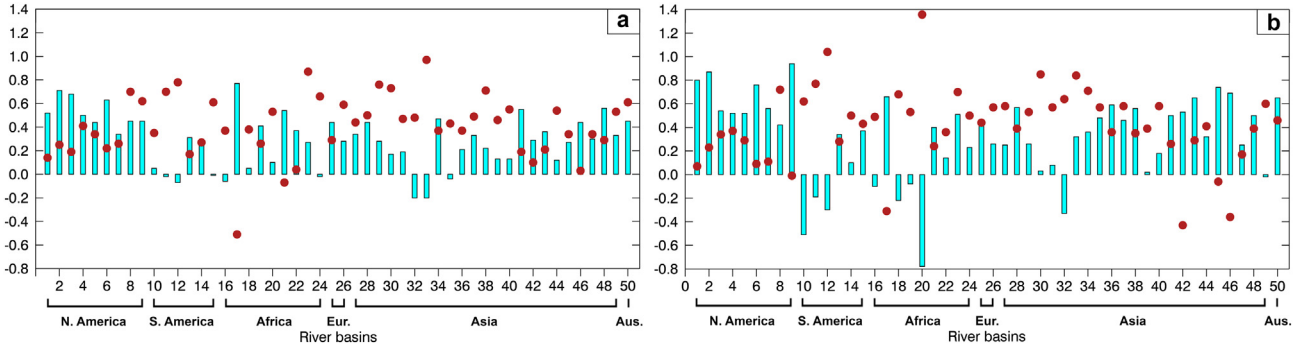

Fig. 5. a) Regression coefficients between the severity of drought episodes identified with the $SPI1_{MSWEP}$ and associated severity of the $SPI1_{PLO}$ (light blue bars) and $SPI1_{PLT}$ (brown dots). b) Same analysis but for the 3-month temporal scale. All results are statistically significant at $p < 0.05$. The X-axis identifies the river basins according to the numbers in Table 2.

one of the world regions with the highest evaporation recycling ratio, plays a key role in precipitation (Worden et al., 2021) and the modulation of drought severity within its borders. We focused on the Lake Chad and Zambezi (Niger, Orange) river basins, where a positive (negative) influence was found between oceanic (terrestrial) severity on the $SPI1_{MSWEP}$ drought episode severity. For the severity of drought episodes identified with the $SPI3_{MSWEP}$, some of the signs of the coefficients change, with more basins showing a negative weight of the $SPI3_{PLO}$ drought severity in the regression equation.

In Europe, the severity of drought episodes that affected the Danube Basin is mostly determined by the severity of the SPI1-3_{PLO}, while that for the Dnieper Basin is mostly determined by the severity of SPI1-3_{PLT}. For 22 of the 25 Asian river basins, both $SPI1_{PLO}$ and $SPI1_{PLT}$ positively influenced the severity of drought events, and in 17 river basins, the effect of the severity resulting from the $SPI1_{PLT}$ was higher. This result was expected after the previous analyses. Moreover, in Northeast Asia, including the Baikal, Lena, and Indigirka river basins, the opposite is true, with the severity of $SPI1_{PLT}$ further positively determining the severity of drought episodes and the $SPI1_{PLO}$ negatively determining the severity. At a 3-month temporal scale, these results are maintained only for Baikal and observed for Hwang-Ho. Finally, the severity of drought episodes in the Murray-Darling River Basin was positively determined by both the SPI1-3_{PLO} and SPI1-3_{PLT}, and it was determined at 1 month mostly by $SPI1_{PLT}$ and at 3 months by $SPI3_{PLO}$, suggesting a lagged memory on the influence of rainfall deficit from oceanic origin on drought severity.

3.3. Copulas and conditional probability analysis

The copula model with the lowest AIC value among the fitted models is shown in Table S1, which was used for the analysis of the pairs (SPI_{MSWEP}, SPI_{PLO}) and (SPI_{MSWEP}, SPI_{PLT}) for each basin. The results regarding the goodness-of-fit of the chosen copulas are shown in Fig. S8. In most cases, the *p*-values are >0.05, which supports the hypothesis that the selected copulas fit well with the data. Thus, as explained in Section 2.3.3, a conditional probability analysis of drought severity based on a copula approach was performed for the studied pairs at temporal scales of 1 month (Fig. 6) and 3 months (Fig. 7). The thresholds used for the analysis are listed in Table 2. River basins on the American continent with the highest conditional probabilities of dry conditions (Z values < -0.84) for ($SPI1_{MSWEP}$, $SPI1_{PLO}$) are located in North America; in particular, the Fraser and Columbia basins have an estimated conditional probability of >70 % (Fig. 6a). Regarding the pair ($SPI1_{MSWEP}$, $SPI1_{PLT}$), the percentages obtained for Yukon, Fraser, and Columbia were lower (Fig. 6b), confirming that these river basins are more prone to drought conditions induced by the reduction in oceanic moisture contribution to precipitation. In contrast, the percentage of the conditional probability of a dry $SPI1_{MSWEP}$ under a dry $SPI1_{PLT}$ increased in the Colorado, Rio Grande, and Saskatchewan-Nelson basins. In South America, the conditional probability of real and oceanic origin dry conditions varies from 30 to 60 %, with the lowest probabilities obtained for the Orinoco and the highest obtained for the San Francisco and Colorado-SA river basins. When the analysis is performed considering the SPI_{PLT}, high estimated conditional probabilities are found in all South American basins, except for the Orinoco and Colorado-SA river basins. In Africa, Europe, and Asia, the major differences in the conditional probabilities between the $SPI1_{PLO}$ and $SPI1_{PLT}$ are observed in the river basins located in the south of Africa, northern Eurasia, and Southeast Asia, where dryness from terrestrial water supply deficit points to a higher conditional probability given the $SPI1_{PLT}$ drought conditions.

The estimated conditional probabilities of severe and extreme drought conditions (Z values < -1.28) at the 1-month temporal scale are shown in Fig. 6c (for $SPI1_{PLO}$) and Fig. 6d (for $SPI1_{PLT}$). For the $SPI1_{PLO}$, the probability is greater in North America than in the South American river basins and greater in western Eurasia basins than in North and Northeast Asia. In addition, a high probability of concurrent observations of severe and extreme drought conditions is observed according to the $SPI1_{MSWEP}$ and $SPI1_{PLO}$ in Murray-Darling (>70 %). For the $SPI1_{PLT}$ (Fig. 6d), an increase in the conditional probability with respect to $SPI1_{PLO}$ was found in almost all the basins of South America, in Saskatchewan-Nelson and Colorado in North America, in the Dnieper in Europe, and in several Asian river basins, such as the Volga, N. Dvina, Yenisey, Ob, Baikal, Lena, Hwang Ho, Ganges and Brahmaputra, and Yangtze, among others. This finding indicates a stronger dependence on severe and extreme drought conditions in these basins based on the occurrence of severe and extreme droughts of terrestrial origin.

The estimated conditional probability (in percentage) of achieving an extreme drought according to the $SPI1_{MSWEP}$ and $SPI1_{PLO}$ and the $SPI1_{MSWEP}$ and $SPI1_{PLT}$ are shown in Fig. 6e and f, respectively. The probabilities obtained for the $SPI1_{MSWEP}$ and $SPI1_{PLO}$ are very heterogeneous among the river basins of North America, ranging from 10 to 20 % in Saskatchewan-Nelson to 60–70 % in St. Lawrence and Columbia. When analyzing the influence of the $SPI1_{PLT}$, the results show lower percentages than those calculated considering the $SPI1_{PLO}$ in six of the nine river basins of North America, which confirms the crucial role of moisture deficit from the oceanic region on the occurrence of extreme drought. Indeed, oceanic forcing has been linked to multiyear droughts in North America (Seager and Hoerling, 2014), although recent findings have also described the importance of decreased moisture transport from upwind land areas associated with reduced evapotranspiration and upwind dry soil moisture with the amplification of droughts across North America (Herrera-Estrada and Diffenbaugh, 2020). In South America, the results show great differences in the estimated conditional probability of extreme drought according to the $SPI1_{PLO}$, with values from 10 to 20 % for Orinoco and 40–50 % for La Plata (Fig. 6e). The percentages obtained with the $SPI1_{PLT}$ (Fig. 6f) were higher or remained the same as those obtained with the $SPI1_{PLO}$, except for the Colorado-SA River Basin, where the values were lower. Concerning selected catchments in Africa, the percentages were higher for the $SPI1_{PLT}$, except for Lake Chad and Jubba-Shebelle.

In Europe and Asia, the conditional probabilities of extreme drought according to the $SPI1_{MSWEP}$ given the drought conditions of both the $SPI1_{PLO}$ (Fig. 6e) and $SPI1_{PLT}$ (Fig. 6f) seemed to be lower than those identified for previous drought categories, as described above. For the $SPI1_{PLO}$, conditional probabilities exceeding 50 % were only observed in the Danube, Dnieper, Amu Darya, and Amur basins, while the lowest probabilities (10–20 %) were observed in the Baikal and Indigirka basins. For the $SPI1_{PLT}$, the estimated probabilities were generally higher for each river basin, with values between 60 and 70 % for the Danube, Dnieper, Tigris-Euphrates, N. Dvina, and Lena and between 50 and 60 % for Ili, Ob, and Amur. Among the Southeast Asian river basins, the estimated conditional probability of extreme drought was higher for the $SPI1_{PLO}$ in the Mekong River Basin (Fig. 6e, f). Finally, in the Murray-Darling River Basin, in addition to other categories of the SPI, a deficit in the oceanic component of precipitation seems to be more associated with the extreme drought conditions identified with the $SPI1_{MSWEP}$ than with a deficit in the terrestrial component.

The results for the pairs ($SPI3_{MSWEP}$, $SPI3_{PLO}$) and ($SPI3_{MSWEP}$, $SPI3_{PLT}$) are shown in Fig. 7. At this SPI time scale, we avoid flash droughts, which are frequent at the temporal scale of 1 month. Thus, the 3 month time scale permitted the assessment of the conditional probability between more realistic drought conditions. For drought conditions ($Z < -0.84$), the highest percentage of conditional probability according to the $SPI3_{PLO}$ values occurred in the basins of North America, South Africa, Europe, and Northwest Asia and the Murray-Darling Basin in Australia (Fig. 7a). For the $SPI3_{PLT}$, higher conditional probabilities are achieved in those basins located in Europe (Dnieper, 70–80 %), and all basins in North and Northeast Asia exceed 50 %, with N. Dvina and Yenisey presenting >70 % (Fig. 7b). The high probability (>70 %) in the La Plata Basin of South America, the Limpopo and Orange basins in southern Africa, and the Murray-Darling Basin in Australia also indicates that the PLT deficit is highly coincident with the occurrence of dry conditions. The probabilities decreased with increases in drought severity, as can be observed in Fig. 7c to f. Under extreme drought conditions (Fig. 7e, f), the percentages were particularly high (60–70 %) for the $SPI3_{PLO}$ in the Columbia, Mississippi, and St. Lawrence

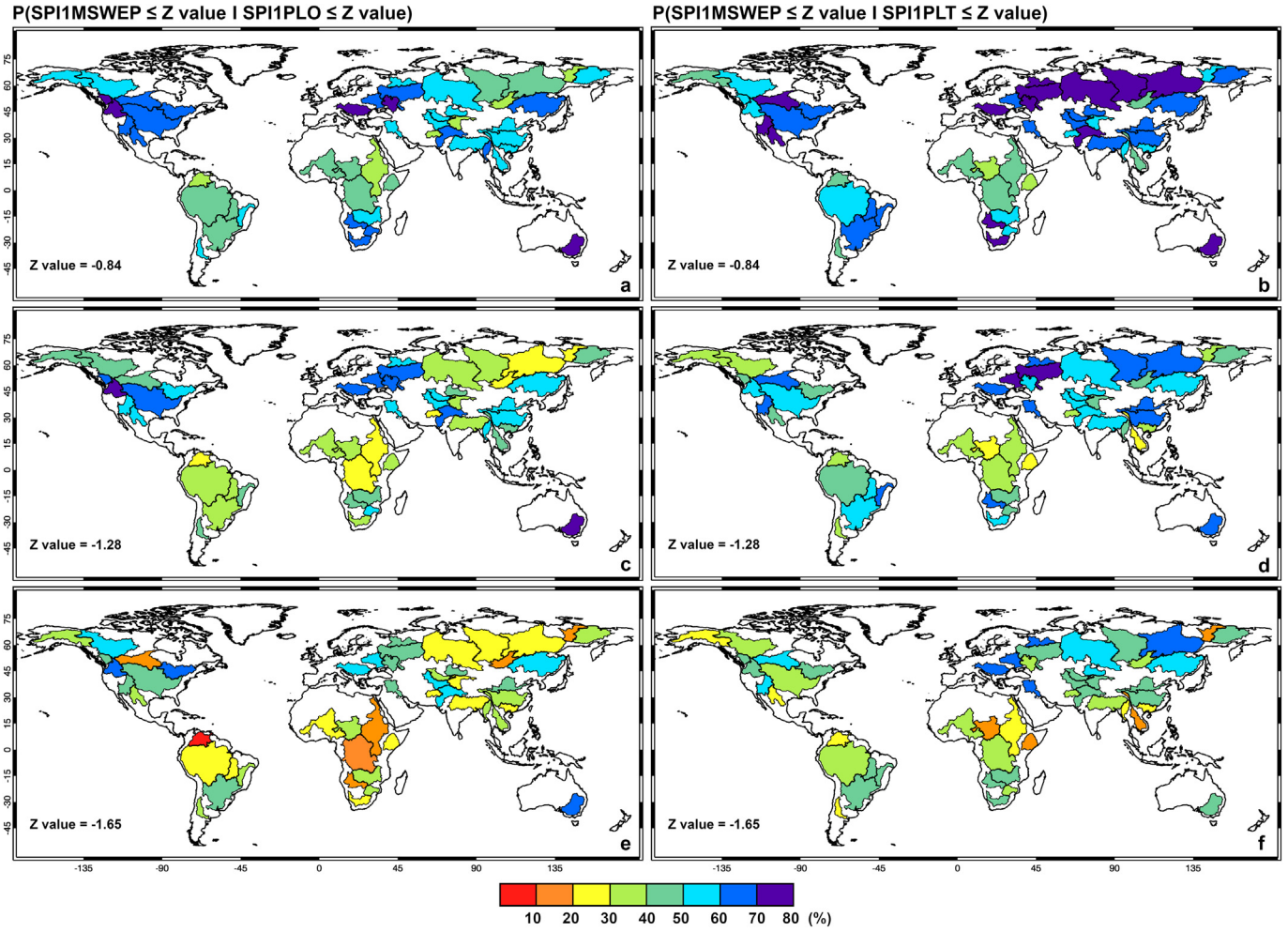

Fig. 6. Estimated conditional probability (in percentage) of experiencing drought (Z value < −0.84), severe and extreme drought (Z value < −1.28), and extreme drought (Z value < −1.65) according to the $SPI1_{MSWEP}$, given the corresponding dry conditions regarding the $SPI1_{PLO}$ (left panel, a, c, e) and $SPI1_{PLT}$ (right panel, b, d, f). Period 1980–2018.

River basins in North America; Limpopo in southern Africa; Amu Darya in Asia; and Murray Darling in Australia. Also under extreme drought conditions, the $SPI3_{PLT}$ is highly concurrent with the $SPI3_{MSWEP}$ in the Saskatchewan-Nelson (70–80 %) in North America, Limpopo (70–80 %) in southern Africa, and the Volga and Hwang Ho basins in Asia (60–70 %).

4. Discussion

In this study we show the climatological percentage of PLO and PLT that contributes to precipitation over each 50 major world river basins (Fig. 2). According to the results, PLT is greater than PLO over the major number of basins, particularly in those of high latitudes of Asia and humid tropical regions of South America and Africa. These are mostly energy-limited regions, where precipitation is highly modulated by moisture fluxes resulting from evapotranspiration and its transport across the continent (McVicar et al., 2012). Bosilovich and Chern (2006) also argue that when precipitation is high, recycling increases and the contribution from external sources decreases, resulting in a negative relationship between the contribution of humidity from oceanic sources and precipitation. In addition, PLO and PLT seem to be modulated by the climatological atmospheric circulation patterns, and dynamical conditions. In North America the higher correlations between PLO and P_{MSWEP} occur in the western basins, where moisture transport from the Pacific (Fig. S2) is often modulated by mechanisms such as atmospheric rivers (Neiman et al., 2008; Gershunov et al., 2019), thus leading to precipitation over western North America (Gimeno et al., 2020), where >50 % of PL is explained by PLO, as shown in Fig. 2. On the contrary, the major relationship between PLT and P_{MSWEP} in the Mississippi may be determined by the importance of continental moisture recycling, which is greatest in eastern North America (Bosilovich and Schubert, 2001; van der Ent et al., 2010). Previous studies have assessed the correlation between moisture inflow and recycling over the Mississippi (Sudradjat et al., 2003; Bosilovich and Chern, 2006), and MacKenzie river basins using different methodologies. Other studies have also revealed that in the central and eastern United States, 45–51 % of precipitation comes from the oceans, 35–39 % comes from upwind land regions, and 14–15 % is internally recycled (Herrera-Estrada and Diffenbaugh, 2020).

The higher correlations of P_{MSWEP} with PLT in South American river basins also confirm the crucial role of continental moisture recycling (Zemp et al., 2014; Yang et al., 2019). However, other studies have documented the primary influence of moisture supply from the tropical North and South Atlantic regions (TNA, TSA) on precipitation (Nieto et al., 2008; Drumond et al., 2014; Martinez and Dominguez, 2014). We found similar findings for the African river basins, confirming the stronger relationship of PLT with the precipitation, as documented before by the high precipitation recycling rates across the continent (Pokam et al., 2012). However, the extension and location of the sources for the Niger River basin (Fig. S3) also confirm the direct impact of moisture transport from the South Atlantic and the Gulf of Guinea in West Africa (Lélé et al., 2015; Sorí et al., 2019). Similarly, the Indian Ocean contributes to the dominance of oceanic precipitation in the Jubba-Shebelle basin. We also found the dominant role of terrestrial moisture contribution to precipitation in the Congo River basin, which has been previously well documented (Sorí et al., 2017c,

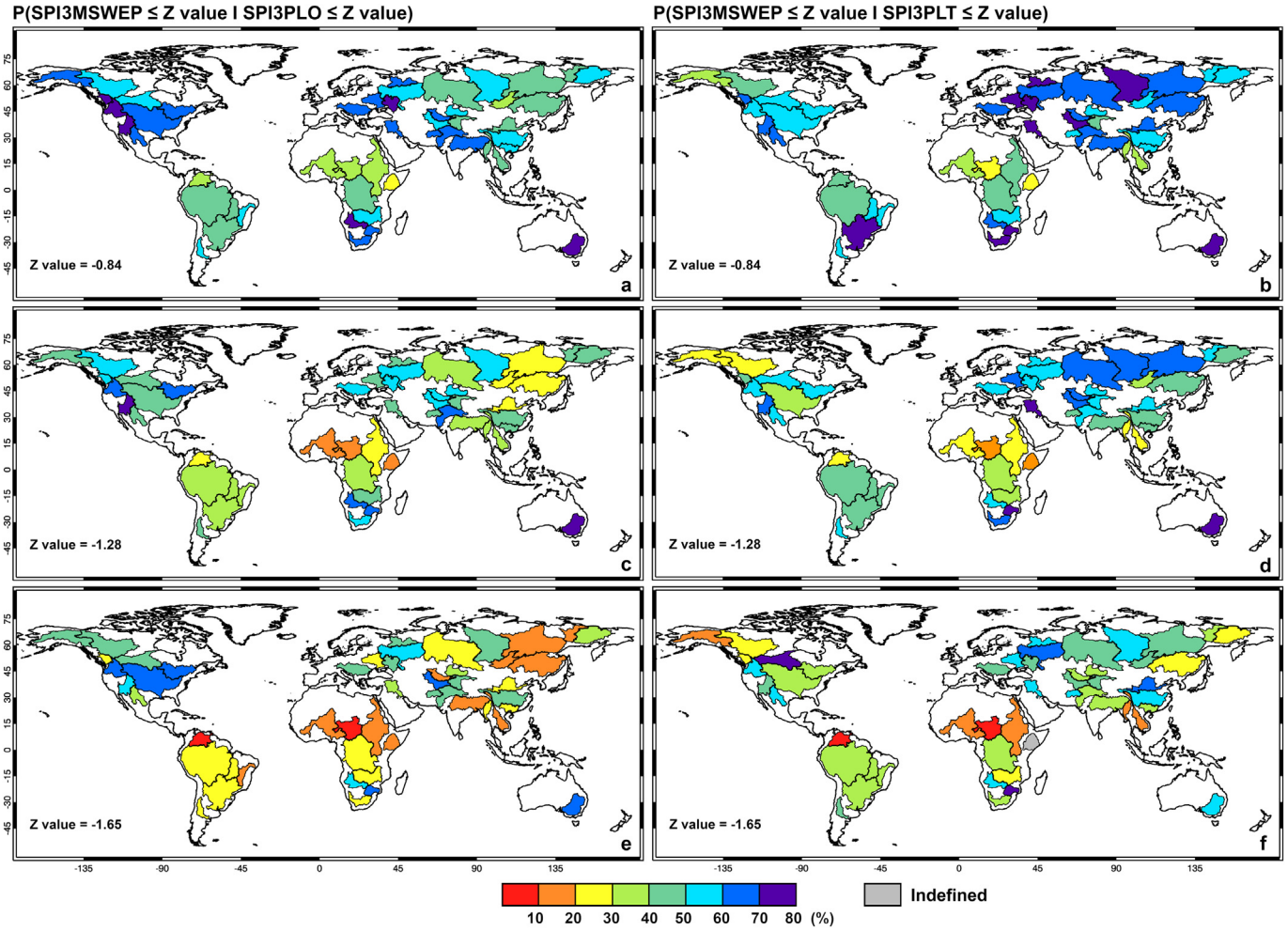

Fig. 7. Estimated conditional probability (in percentage) of experiencing drought (Z value < -0.84), severe and extreme drought (Z value < -1.28), and extreme drought (Z value < -1.65) according to the $SPI3_{MSWEP}$ given the corresponding dry conditions regarding the $SPI3_{PLO}$ (left panel, a, c, e) and $SPI3_{PLT}$ (right panel, b, d, f). Period 1980–2018.

2019; Worden et al., 2021; Te Wierik et al., 2022). The patterns of moisture uptake by air masses that reach the south and southeast river basins (Fig. S5) confirm the crucial role of the Indian Ocean and the East and South China Seas as sources of moisture (Bin et al., 2013; Sorí et al., 2017c). PLO and particularly PLT correlates.

The patterns of (E–P) > 0 for the northern Eurasian basins (Fig. S5) reveal the importance of the land contribution, but also the transport from the Mediterranean and the Atlantic. This result deserves further research to clarify the role of oceanic and terrestrial precipitation origin in the runoff trends already documented for the Siberian watersheds (Berezovskaya et al., 2004; Vasilevskaya et al., 2021). Although the correlation does not imply causality, in general, the high relationship between P_{MSWEP} and PL, PLO and PLT in the basins does confirm the usefulness of Lagrangian precipitation and its components for the attribution of changes that may occur in the hydrological cycle, and lead to the occurrence of extreme events such as droughts.

Despite much progress has been made in recent decades on drought studies, the controlling factors of its occurrence and propagation are still lacking (Wang et al., 2016; Zhang et al., 2022). In this regard, for this study we applied a novel approach in which we estimate dry conditions of oceanic or terrestrial origin in each of the basins studied through the SPI. Concerns have recently been raised about the usefulness of SPI for estimating drought conditions in a global warming context, as it does not address changes in evapotranspiration. However, one of the advantages of the SPI is its simplicity in considering only one variable in its computation, which allowed investigating the role of oceanic and terrestrial dry conditions individually and jointly in the occurrence of droughts, something difficult to achieve with indices involving more variables. Although, in future studies this is something we will take into account, to achieve a more accurate analysis. Our results show the value of each of these components (PLO and PLT), in the characterization of drought conditions in the basins. Dry conditions associated with PLT and PLO deficits are mostly directly associated with the occurrence and severity of drought episodes at one and three months' SPI_{MSWEP} temporal scale, and are consistent with the correlations. As appreciated, in most of the North American river basins the oceanic origin drought conditions have a greater weight in determining the final drought conditions. However, in some basins such as Lake Chad in Africa, drought response to SPI_{PLO} and SPI_{PLT} at both SPI temporal scale is opposite, indicating the primary impact of the oceanic component. Similarly, in other basins, the propagation of dry conditions of oceanic or terrestrial origin from 1 to 3 months, modulate individually the behaviour of drought. This, for example, occurs in the Congo, where the $SPI3_{PLT}$ ($SPI3_{PLO}$) determines positively (negatively) the behaviour of drought. A copula analysis was also used to determine the conditional probability of drought at different ranges of severity between the pairs $SPI1\text{-}3_{MSWEP}$ with $SPI1\text{-}3_{PLO}$ and $SPI1\text{-}3_{MSWEP}$ with $SPI1\text{-}3_{PLT}$. With this analysis, we demonstrated that conditional drought conditions ($SPI1\text{-}3_{MSWEP} < -0.84$) in North America (north of Asia and South America) river basins experience a greater change in probability due to oceanic (terrestrial) origin drought forcing, in comparison with the terrestrial (oceanic) one, which is consistent with the results before discussed. In the Murray Darling river basin, the probabilities differ only under extreme drought conditions

when drought of oceanic origin is more likely to occur jointly with that identified with the SPI_{MSWEP}, confirming the importance of the Indian Ocean as the principal source of moisture. Previous findings also revealed that major southeast Australian droughts were intensified and terminated chiefly by anomalies on the moisture transport from the Ocean (Holgate et al., 2020).

5. Conclusions

The Lagrangian approach previously developed by the authors of this article (Nieto and Gimeno, 2019; Gimeno et al., 2020) allowed for the computation of an estimated Lagrangian precipitation named PL and separated it into precipitation from oceanic (PLO) and terrestrial (PLT) origins over 50 world river basins for the study period 1980–2018. The results revealed:

- A high and statistically significant relationship between precipitation from MSWEP and the PL, PLO, and PLT series in almost all basins.
- In most of the basins, a major amount of PLT prevails, which confirms the importance of continental recycling of precipitation and evaporation as well as moisture exports across the continents as a source of the land-based precipitation origin, which deserves further analysis.
- PLO stands out as the dominant component of precipitation in North American river basins, as well as in others such as the Jubba-Shebelle in Africa, the Danube in Europe, and the Mekong and Si in Southeast Asia. The geographical location and major mechanisms of moisture transport, such as atmospheric rivers and low-level jets, appear to be crucial factors for this result.
- The identification of drought episodes showed a higher number on the 1-month temporal scale of the SPI_{MSWEP} for all basins compared to those obtained on the 3-month temporal scale, especially for the Congo and Amazon, which presented the lowest number of episodes but the highest average severity and duration.
- The SPI1-3_{PLO} and SPI1-3_{PLT} were obtained for each river basin, which allowed us to prove through multiple regressions that both components have a positive effect on the estimation of the severity of drought episodes according to the SPI1-3_{MSWEP} for a large number of river basins.
- The copula analysis revealed major conditional probabilities of drought of oceanic origin in most of the basins of North America, Europe, Northwest and Southeast Asia, and southern Africa. In contrast, the analysis performed with the SPI1-3_{PLT} showed higher probabilities in the river basins located in North and Northeast Asia, South America, and the central and southern regions of Africa. In the Murray basin, the SPI1-3_{PLO} and SPI1-3_{PLT} are highly associated with drought conditions, but when drought severity increases, the correspondence is greater with dry conditions of oceanic origin.

The results of this study have confirmed the usefulness of including the oceanic and terrestrial components of Lagrangian precipitation for characterizing the origin of precipitation over 50 world river basins. Additionally, we have introduced a framework which allows accounting for the underlying role of dry conditions from oceanic and terrestrial origin when investigating the occurrence and severity of droughts in the basins, but also in any other region. The findings also provide opportunities for drought early warning and future research. Research is ongoing to determine the long-term relationships and influence of climate modes of variability on the precipitation from oceanic and terrestrial origin, in order to provide a deeper understanding of the hydrological cycle characteristics and vegetation dynamics at the river basin scale.

Supplementary data to this article can be found online at https://doi.org/10.1016/j.scitotenv.2022.160288.

CRediT authorship contribution statement

Rogert Sorí, Luis Gimeno, Luis Gimeno-Sotelo, Raquel Nieto, and Margarida L.R. Liberado conceived and designed the manuscript. Rogert Sorí, Luis Gimeno-Sotelo, Milica Stojanovic, Albenis Pérez-Alarcón, and José Carlos Fernández-Alvarez performed the data curation, formal analysis, investigation, methodology, validation and visualization. Rogert Sorí and Luis Gimeno-Sotelo wrote the manuscript. All the authors reviewed the manuscript.

Funding

The CRUE-CSIC agreement with Elsevier supported the Open Access funding of this study. This research was financed by the LAGRIMA and SETESTRELO projects (grants no. RTI2018-095772-B-I00 and PID2021-122314OB-I00, respectively) funded by the Ministerio de Ciencia, Innovación y Universidades, Spain. Partial support was also obtained from the Xunta de Galicia, Consellería de Cultura, Educación e Universidade, under project ED431C 2021/44 “Programa de Consolidación e Estructuración de Unidades de Investigación Competitivas”.

Data availability

Data will be made available on request.

Declaration of competing interest

The authors declare no conflict of interest.

Acknowledgments

Rogert Sorí, Milica Stojanovic, and José Carlos Fernández-Alvarez acknowledge the support of grants no. ED481B-2019/070, ED481B-2021/134, and ED481A-2020/193 from the Xunta of Galicia, respectively. Luis Gimeno-Sotelo and Albenis Pérez-Alarcón thank a PhD grant from the University of Vigo.

References

Algarra, I., Eiras-Barca, J., Miguez-Macho, G., Nieto, R., Gimeno, L., 2019. On the assessment of the moisture transport by the Great Plains low-level jet. Earth Syst. Dynam. 10 (107–119), 2019. https://doi.org/10.5194/esd-10-107-2019.

Agnew, C.T., 2022. Using the SPI to identify drought. 2000Drought Netw. News. 12, pp. 6–12 available at: http://digitalcommons.unl.edu/droughtnetnews/1 (last access: 10 March 2022).

Akaike, H., 1974. A new look at the statistical model identification. IEEE Trans. Autom. Control 19 (6), 716–723.

Beck, H.E., Wood, E.F., Pan, M., Fisher, C.K., Miralles, D.M., van Dijk, A.I.J.M., McVicar, T.R., Adler, R.F., 2019. MSWEP V2 global 3-hourly 0.1° precipitation: methodology and quantitative assessment. Bull. Am. Meteorol. Soc. 100 (3), 473–500.

Berezovskaya, S., Yang, D., Kane, D.L., 2004. Compatibility analysis of precipitation and runoff trends over the large Siberian watersheds. Geophys. Res. Lett. 31, L21502. https://doi.org/10.1029/2004GL021277.

Bin, C., Xiang-De, X., Tianliang, Z., 2013. Main moisture sources affecting lower Yangtze River basin in boreal summers during 2004–2009. Int. J. Climatol. 33, 1035–1046. https://doi.org/10.1002/joc.3495.

Bosilovich, M.G., Schubert, S.D., 2001. Precipitation recycling over the Central United States diagnosed from the GEOS-1 data assimilation system. J. Hydrometeorol. 2 (1), 26–35.

Bosilovich, M.G., Chern, J., 2006. Simulation of water sources and precipitation recycling for the MacKenzie, Mississippi, and Amazon River basins. J. Hydrometeorol. 7 (3), 312–329.

Brubaker, K.L., Dirmeyer, P.A., Sudradjat, A., Levy, B.S., Bernal, F., 2001. A 36-yr Climatological Description of the Evaporative Sources of Warm-Season Precipitation in the Mississippi River Basin. J. Hydrometeorol. 2 (6), 537–557. https://doi.org/10.1175/1525-7541(2001)002<0537:AYCDOT>2.0.CO;2.

Brubaker, K.L., Entekhabi, D., Eagleson, P.S., 1993. Estimation of continental precipitation recycling. J. Clim. 6 (6), 1077–1089 https://journals.ametsoc.org/view/journals/clim/6/6/1520-0442_1993_006_1077_eocpr_2_0_co_2.xml https://journals.ametsoc.org/view/journals/clim/6/6/1520-0442_1993_006_1077_eocpr_2_0_co_2.xml.

Brunner, M.I., Slater, L., Tallaksen, L.M., Clark, M., 2021. Challenges in modeling and predicting floods and droughts: a review. WIREs Water 8, e1520. https://doi.org/10.1002/wat2.1520.

Carvalho, L.M.V., Silva, A.E., Jones, C., et al., 2011. Moisture transport and intraseasonal variability in the South America monsoon system. Clim. Dyn. 36, 1865–1880. https://doi.org/10.1007/s00382-010-0806-2.

Czado, C., 2019. Analyzing dependent data with vine copulas. Lecture Notes in Statistics. Springer.

Chiang, F., Mazdiyasni, O., AghaKouchak, A., 2021. Evidence of anthropogenic impacts on global drought frequency, duration, and intensity. Nat. Commun. 12, 2754. https://doi.org/10.1038/s41467-021-22314-w.

Christidis, N., Stott, P.A., 2021. The influence of anthropogenic climate change on wet and dry summers in Europe. Sci. Bull. 66 (8), 813–823. https://doi.org/10.1016/j.scib.2021.01.020.

Ciric, D., Stojanovic, M., Drumond, A., Nieto, R., Gimeno, L., 2016. Tracking the origin of moisture over the Danube River Basin using a lagrangian approach. Atmosphere 7, 162. https://doi.org/10.3390/atmos7120162.

Cook, K.H., Vizy, E.K., 2010. Hydrodynamics of the Caribbean low-level jet and its relationship to precipitation. J. Clim. 23 (6), 1477–1494.

Cook, B.I., Seager, R., Williams, A.P., Puma, M.J., McDermid, S., Kelley, M., Nazarenko, L., 2019. Climate change amplification of natural drought variability: the historic mid-twentieth-century North American drought in a warmer world. J. Clim. 32 (17), 5417–5436.

Dee, D.P., et al., 2011. The ERA-interim reanalysis: configuration and performance of the data assimilation system. Q. J. R. Meteorol. Soc. 137, 553–597. https://doi.org/10.1002/qj.828.

Dey, D., Döös, K., 2021. Tracing the origin of the South Asian summer monsoon precipitation and its variability using a novel lagrangian framework. J. Clim. 34 (21), 8655–8668.

Dirmeyer, P.A., Brubaker, K.L., 1999. Contrasting evaporative moisture sources during the drought of 1988 and the flood of 1993. J. Geophys. Res. 104 (D16), 19383–19397. https://doi.org/10.1029/1999JD900222.

Drumond, A., Marengo, J., Ambrizzi, T., Nieto, R., Moreira, L., Gimeno, L., 2014. The role of the Amazon Basin moisture in the atmospheric branch of the hydrological cycle: a lagrangian analysis. Hydrol. Earth Syst. Sci. 18, 2577–2598. https://doi.org/10.5194/hess-18-2577-2014.

Drumond, A., Stojanovic, M., Nieto, R., Vicente-Serrano, S.M., Gimeno, L., 2019. Linking anomalous moisture transport and drought episodes in the IPCC reference regions. Bull. Am. Meteorol. Soc. 100 (8), 1481–1498.

Dyer, E.L.E., Jones, D.B.A., Nusbaumer, J., Li, H., Collins, O., Vettoretti, G., Noone, D., 2017. Congo Basin precipitation: assessing seasonality, regional interactions, and sources of moisture. J. Geophys. Res. Atmos. 122, 6882–6898. https://doi.org/10.1002/2016JD026240.

Eltahir, E.A.B., Bras, R.L., 1994. Precipitation recycling in the Amazon basin. Q. J. R. Meteorol. Soc. 120, 861–880. https://doi.org/10.1002/qj.49712051806.

Findell, K.L., Keys, P.W., van der Ent, R.J., Lintner, B.R., Berg, A., Krasting, J.P., 2019. Rising temperatures increase importance of oceanic evaporation as a source for continental precipitation. J. Clim. 32 (22), 7713–7726.

Frank, A., Seibert, P., Wotawa, G., 2005. Technical note: the Lagrangian particle dispersion model FLEXPART version 6.2. Atmos. Chem. Phys. 5, 2461–2474.

Gershunov, A., Shulgina, T., Clemesha, R.E.S., et al., 2019. Precipitation regime change in Western North America: the role of atmospheric rivers. Sci. Rep. 9, 9944. https://doi.org/10.1038/s41598-019-46169-w.

Gimeno, L., Drumond, A., Nieto, R., Trigo, R.M., Stohl, A., 2010. On the origin of continental precipitation. Geophys. Res. Lett. 37, L13804. https://doi.org/10.1029/2010GL043712.

Gimeno, L., Stohl, A., Trigo, R.M., Dominguez, F., Yoshimura, K., Yu, L., Drumond, A., Durán-Quesada, A.M., Nieto, R., 2012. Oceanic and terrestrial sources of continental precipitation. Rev. Geophys. 50, RG4003. https://doi.org/10.1029/2012RG000389.

Gimeno, L., Nieto, R., Sorí, R., 2020. The growing importance of oceanic moisture sources for continental precipitation. npj Clim. Atmos. Sci. 3, 27. https://doi.org/10.1038/s41612-020-00133-y.

Guan, B., Waliser, D.E., 2015. Detection of atmospheric rivers: evaluation and application of an algorithm for global studies. J. Geophys. Res. Atmos. 120, 12514–12535. https://doi.org/10.1002/2015JD024257.

Guo, C., Bai, Z., Shi, X., Chen, X., Chadwick, D., Strokal, M., Zhang, F., Ma, L., Chen, X., 2021. Challenges and strategies for agricultural green development in the Yangtze River Basin. J. Integr. Environ. Sci. 18 (1), 37–54. https://doi.org/10.1080/1943815X.2021.1883674.

Hao, Z., Singh, V.P., Xia, Y., 2018. Seasonal drought prediction: advances, challenges, and future prospects. Rev. Geophys. 56, 108–141. https://doi.org/10.1002/2016RG000549.

Herrera-Estrada, J.E., Diffenbaugh, N.S., 2020. Landfalling droughts: global tracking of moisture deficits from the oceans onto land. Water Resour. Res. 56, e2019WR026877. https://doi.org/10.1029/2019WR026877.

Holgate, C.M., Van Dijk, A.I.J.M., Evans, J.P., Pitman, A.J., 2020. Local and remote drivers of southeast Australian drought. Geophys. Res. Lett. 47, e2020GL090238. https://doi.org/10.1029/2020GL090238.

Horton, R.E., 1932. Drainage-basin characteristics. Eos Trans. AGU 13 (1), 350–361. https://doi.org/10.1029/TR013i001p00350.

Huang, W., Prokhorov, A., 2014. A goodness-of-fit test for copulas. Econ. Rev. 33 (7), 751–771.

Keune, J., Miralles, D.G., 2019. A precipitation recycling network to assess freshwater vulnerability: challenging the watershed convention. Water Resour. Res. 55, 9947–9961. https://doi.org/10.1029/2019WR025310.

Keys, P.W., Wang-Erlandsson, L., Gordon, L.J., 2016. Revealing invisible water: moisture recycling as an ecosystem service. PLoS ONE 11 (3), e0151993. https://doi.org/10.1371/journal.pone.0151993.

Lélé, M.I., Leslie, L.M., Lamb, P.J., 2015. Analysis of low-level atmospheric moisture transport associated with the West African monsoon. J. Clim. 28 (11), 4414–4430.

Levin, N.E., Zipser, E.J., Cerling, T.E., 2009. Isotopic composition of waters from Ethiopia and Kenya: insights into moisture sources for eastern Africa. J. Geophys. Res. 114, D23306. https://doi.org/10.1029/2009JD012166.

Martinez, J.A., Dominguez, F., 2014. Sources of atmospheric moisture for the La Plata River Basin. J. Clim. 27 (17), 6737–6753.

Mckee, T.B., Doesken, N.J., Kleist, J., 1993. The Relationship of Drought Frequency and Duration to Time Scales. Proceedings of the Eighth Conference on Applied Climatology. American Meteorological Society, Jan17-23, 1993, Anaheim CA, pp. 179–184.

McVicar, T.R., et al., 2012. Global review and synthesis of trends in observed terrestrial near-surface wind speeds: Implications for evaporation. J. Hydrol. 416-417, 182–205. https://doi.org/10.1016/j.jhydrol.2011.10.024.

Montini, T.L., Jones, C., Carvalho, L.M.V., 2019. The South American low-level jet: a new climatology, variability, and changes. J. Geophys. Res.-Atmos. 124, 1200–1218. https://doi.org/10.1029/2018JD029634.

Nagler, T., Schepsmeier, U., Stoeber, J., Brechmann, E.C., Graeler, B., Erhardt, T., 2020. VineCopula: statistical inference of vine copulas. URL https://CRAN.R-project.org/package=VineCopula-R-package-version-2.4.1.

Neiman, P.J., Ralph, F.M., Wick, G.A., Lundquist, J.D., Dettinger, M.D., 2008. Meteorological characteristics and overland precipitation impacts of atmospheric rivers affecting the west coast of North America based on eight years of SSM/I satellite observations. J. Hydrometeorol. 9 (1), 22–47.

Nelsen, R.B., 2006. An Introduction to Copulas. Springer Science & Business Media.

Nieto, R., Gimeno, L., Trigo, R.M., 2006. A Lagrangian identification of major sources of Sahel moisture. Geophys. Res. Lett. 33, L18707. https://doi.org/10.1029/2006GL027232.

Nieto, R., Gallego, D., Trigo, R., Ribera, P., Gimeno, L., 2008. Dynamic identification of moisture sources in the Orinoco basin in equatorial South America. Hydrol. Sci. J. 53 (3), 602–617. https://doi.org/10.1623/hysj.53.3.602.

Nieto, R., Gimeno, L., 2019. A database of optimal integration times for lagrangian studies of atmospheric moisture sources and sinks. Sci. Data 6, 59.

Nieto, R., Gimeno, L., 2021. Addendum: a database of optimal integration times for lagrangian studies of atmospheric moisture sources and sinks. Sci. Data 8, 130. https://doi.org/10.1038/s41597-021-00902-1.

Papritz, L., Hauswirth, D., Hartmuth, K., 2022. Moisture origin, transport pathways, and driving processes of intense wintertime moisture transport into the Arctic. Weather Clim. Dynam. 3, 1–20. https://doi.org/10.5194/wcd-3-1-2022.

Pascale, S., Kapnick, S.B., Delworth, T.L., et al., 2021. Natural variability vs forced signal in the 2015–2019 Central American drought. Clim. Chang. 168, 16. https://doi.org/10.1007/s10584-021-03228-4.

Pokam et al., 2012. W.M. Pokam L.A.T. Djiotang F.K. Mkankam Atmospheric water vapor transport and recycling in Equatorial Central Africa through NCEP/NCAR reanalysis data. Clim. Dyn. 38, 1715–1729. doi: doi:10.1007/s00382-011-1242-7. 2012.

Pouyaei, A., Choi, Y., Jung, J., Mousavinezhad, S., Momeni, M., Song, C.-H., 2022. Investigating the long-range transport of particulate matter in East Asia: introducing a new Lagrangian diagnostic tool. Atmos. Environ. 278, 119096. https://doi.org/10.1016/j.atmosenv.2022.119096.

Pu, B., Cook, K.H., 2010. Dynamics of the West African Westerly Jet. J. Clim. 23 (23), 6263–6276. https://doi.org/10.1175/2010JCLI3648.1.

R Core Team, 2022. R: A Language And Environment for Statistical Computing. R Foundation for Statistical Computing, Vienna, Austria https://www.R-project.org/.

Seager, R., Hoerling, M., 2014. Atmosphere and ocean origins of North American droughts. J. Clim. 27 (12), 4581–4606. https://doi.org/10.1175/JCLI-D-13-00329.1.

Shapiro, A.C., Grantham, H.S., Aguilar-Amuchastegui, N., Murray, N.J., Gond, V., Bonfils, D., Rickenbach, O., 2021. Forest condition in the Congo Basin for the assessment of ecosystem conservation status. Ecol. Indic. 122, 107268. https://doi.org/10.1016/j.ecolind.2020.107268.

Shemyakin, A., Kniazev, A., 2017. Introduction to Bayesian Estimation And Copula Models of Dependence. John Wiley & Sons.

Shi, Y., Jiang, Z., Liu, Z., Li, L., 2020. A Lagrangian analysis of water vapor sources and pathways for precipitation in East China in different stages of the East Asian summer monsoon. J. Clim. 33 (3), 977–992.

Sorí, R., Nieto, R., Vicente-Serrano, S.M., Drumond, A., Gimeno, L., 2017. A Lagrangian perspective of the hydrological cycle in the Congo River basin. Earth Syst. Dynam. 8 (653–675), 2017. https://doi.org/10.5194/esd-8-653-2017.

Sorí, R., Nieto, R., Drumond, A., Vicente-Serrano, S.M., Gimeno, L., 2017b. The atmospheric branch of the hydrological cycle over the Indus, Ganges, and Brahmaputra river basins. Hydrol. Earth Syst. Sci. 21, 6379–6399. https://doi.org/10.5194/hess-21-6379-2017.

Sorí, R., Nieto, R., Drumond, A., Gimeno, L., 2017c. The Niger River basin moisture sources: a Lagrangian analysis. Atmosphere 8, 38. https://doi.org/10.3390/atmos8020038.

Sorí, R., Nieto, R., Drumond, A., Stojanovic, M., Gimeno, L., 2019. On the connection between atmospheric moisture transport and dry conditions in rainfall climatological zones of the Niger River basin. Water 11, 622. https://doi.org/10.3390/w11030622.

Stohl, A., James, P., 2004. A Lagrangian analysis of the atmospheric branch of the global water cycle. Part I: method description, validation, and demonstration for the August 2002 flooding in central Europe. J. Hydrometeorol. 5, 656–678.

Stohl, A., James, P., 2005. A Lagrangian analysis of the atmospheric branch of the global water cycle. Part II: moisture transports between Earth's ocean basins and river catchments. J. Hydrometeorol. 6 (6), 961–984.

Stojanovic, M., Drumond, A., Nieto, R., Gimeno, L., 2017. Moisture transport anomalies over the Danube River Basin during two drought events: a Lagrangian analysis. Atmosphere 8, 193. https://doi.org/10.3390/atmos8100193.

Sudradjat, A., Brubaker, K.L., Dirmeyer, P.A., 2003. Interannual variability of surface evaporative moisture sources of warm-season precipitation in the Mississippi River basin. J. Geophys. Res. 108, 8612. https://doi.org/10.1029/2002JD003061, D16.

Svoboda, M., Hayes, M., Wood, D., 2012. Standardized Precipitation Index User Guide. World Meteorological Organization, Geneva WMO Rp. 1090, 24 pp.

Tootoonchi, F., Sadegh, M., Haerter, J.O., Räty, O., Grabs, T., Teutschbein, C., 2022. Copulas for hydroclimatic analysis: a practice-oriented overview. Wiley Interdiscip. Rev. Water 9 (2), e1579. https://doi.org/10.1002/wat2.1579.

Trenberth, K.E., Fasullo, J.T., Mackaro, J., 2011. Atmospheric moisture transports from ocean to land and global energy flows in reanalyses. J. Clim. 24, 4907–4924. https://doi.org/10.1175/2011JCLI4171.1.

TWAP (Transboundary Waters Assessment Programme), 2022. http://twap-rivers.org/#home Last access on 13 March 2022.

Tso, C.-H.-M., Monteith, D., Scott, T., Watson, H., Dodd, B., Pereira, M.G., Henrys, P., Hollaway, M., Rennie, S., Lowther, A., Watkins, J., Killick, R., Blair, G., 2022. The evolving role of weather types on rainfall chemistry under large reductions in pollutant emissions. Environ. Pollut. 299, 118905. https://doi.org/10.1016/j.envpol.2022.118905.

United Nations Office for Disaster Risk Reduction, 2021. GAR Special Report on Drought 2021 Geneva. ISBN: 9789212320274.
Vasilevskaya, L.N., Lisina, I.A., Vasilevskii, D.N., 2021. Influence of large-scale atmospheric processes on seasonal runoff of large Siberian Rivers. Russ. Meteorol. Hydrol. 46, 674–682. https://doi.org/10.3103/S1068373921100046.
van der Ent, R.J., Savenije, H.H.G., Schaefli, B., Steele-Dunne, S.C., 2010. Origin and fate of atmospheric moisture over continents. Water Resour. Res. 46, W09525. https://doi.org/10.1029/2010WR009127.
Vázquez, M., Nieto, R., Liberato, M.L.R., Gimeno, L., 2020. Atmospheric moisture sources associated with extreme precipitation during the peak precipitation month. Weather Clim. Extremes 30, 100289. https://doi.org/10.1016/j.wace.2020.100289.
Vicente-Serrano, S.M., Beguería, S., Lorenzo-Lacruz, J., Camarero, J.J., López-Moreno, J.I., Azorin-Molina, C., Revuelto, J., Morán-Tejeda, E., Sanchez-Lorenzo, A., 2012. Performance of drought indices for ecological, agricultural, and hydrological applications. Earth Interact. 16 (10), 1–27.
Vicente-Serrano, S.V., 2021. La evolución de los estudios sobre sequías climáticas en España en las últimas décadas. Geographicalia 73. https://doi.org/10.26754/ojs_geoph/02108380 7- 3.
Viste, E., Sorteberg, A., 2013. Moisture transport into the Ethiopian highlands. Int. J. Climatol. 33, 249–263. https://doi.org/10.1002/joc.3409.
Vuille, M., Burns, S.J., Taylor, B.L., Cruz, F.W., Bird, B.W., Abbott, M.B., Kanner, L.C., Cheng, H., Novello, V.F., 2012. A review of the South American monsoon history as recorded in stable isotopic proxies over the past two millennia. Clim. Past 8, 1309–1321. https://doi.org/10.5194/cp-8-1309-2012.
Wang, C., 2007. Variability of the Caribbean Low-level Jet and its relations to climate. Clim. Dyn. 29, 411–422. https://doi.org/10.1007/s00382-007-0243-z.
Wang, W., Ertsen, M.W., Svoboda, M.D., Hafeez, M., 2016. Propagation of drought: from meteorological drought to agricultural and hydrological drought. Adv. Meteorol., 6547209 https://doi.org/10.1155/2016/6547209 5 pp.
Wanzeler da Costa, C.P., Satyamurty, P., 2016. Inter-hemispheric and inter-zonal moisture transports and monsoon regimes. Int. J. Climatol. 36, 4705–4722. https://doi.org/10.1002/joc.4662.
White, H., 1982. Maximum likelihood estimation of misspecified models. Econometrica 1–25.
Winschall, A., Pfahl, S., Sodemann, H., Wernli, H., 2014. Comparison of Eulerian and Lagrangian moisture source diagnostics – the flood event in eastern Europe in May 2010. Atmos. Chem. Phys. 14, 6605–6619. https://doi.org/10.5194/acp-14-6605-2014.
Wittmann, F., Junk, W.J., 2016. Amazon River Basin. In: Finlayson, C., Milton, G., Prentice, R., Davidson, N. (Eds.), The Wetland Book. Springer, Dordrecht https://doi.org/10.1007/978-94-007-6173-5_83-2.
Worden, S., Fu, R., Chakraborty, S., Liu, J., Worden, J., 2021. Where does moisture come from over the Congo Basin? J. Geophys. Res. Biogeosci. 126, e2020JG006024. https://doi.org/10.1029/2020JG006024.
Wu, S.-Y., Bedaso, Z., 2022. Quantifying the effect of moisture source and transport on the precipitation isotopic variations in northwest Ethiopian Highland. J. Hydrol. 605, 127322. https://doi.org/10.1016/j.jhydrol.2021.127322 ISSN 0022-1694.
Yang, Z., Dominguez, F., 2019. Investigating land surface effects on the moisture transport over South America with a moisture tagging model. J. Clim. 32 (19), 6627–6644.
Yang, R., Zhang, W.K., Gui, S., et al., 2019. Rainy season precipitation variation in the Mekong River basin and its relationship to the Indian and East Asian summer monsoons. Clim. Dyn. 52, 5691–5708. https://doi.org/10.1007/s00382-018-4471-1.
Yu, Y., Notaro, M., Wang, F., et al., 2017. Observed positive vegetation-rainfall feedbacks in the Sahel dominated by a moisture recycling mechanism. Nat. Commun. 8, 1873. https://doi.org/10.1038/s41467-017-02021-1.
Zandonadi-Moura, L., Lima, C.H.R., 2018. Analysis of atmospheric moisture transport to the Upper Paraná River basin. Int. J. Climatol. 38, 5153–5167. https://doi.org/10.1002/joc.5718.
Zemp, D.C., Schleussner, C.-F., Barbosa, H.M.J., van der Ent, R.J., Donges, J.F., Heinke, J., Sampaio, G., Rammig, A., 2014. On the importance of cascading moisture recycling in South America. Atmos. Chem. Phys. 14, 13337–13359. https://doi.org/10.5194/acp-14-13337-2014.
Zhang, X., Hao, Z., Singh, V.P., Zhang, Y., Feng, S., Xu, Y., Hao, F., 2022. Drought propagation under global warming: characteristics, approaches, processes, and controlling factors. Sci. Total Environ. 838 (Part 2), 156021. https://doi.org/10.1016/j.scitotenv.2022.156021.
Zhao, T., Zhao, J., Hu, H., et al., 2016. Source of atmospheric moisture and precipitation over China's major river basins. Front. Earth Sci. 10, 159–170. https://doi.org/10.1007/s11707-015-0497-4.